Performance Optimization and Guidance of a Low-Altitude Skid-To-Turn Vehicle. Part I: Performance Optimization

Miriam E. Dennis*
Anil V. Rao†

University of Florida
Gainesville, FL 32611

The problem of air-to-surface trajectory optimization for a low-altitude skid-to-turn vehicle is considered. The objective is for the vehicle to move level at a low altitude for as long as possible and perform a rapid bunt (negative sensed-acceleration load) maneuver near the final time in order to attain terminal target conditions. The vehicle is modeled as a point mass in motion over a flat Earth, and the vehicle is controlled using thrust magnitude, angle of attack, and sideslip angle. The trajectory optimization problem is posed as a two-phase optimal control problem using a weighted objective function. The work described in this paper is the first part of a two-part sequence on trajectory optimization and guidance of a skid-to-turn vehicle. In both cases, the objective is to minimize the time taken by the vehicle to complete a bunt maneuver subject to the following constraints: dynamic, boundary, state, path, and interior-point event constraints. In the first part of this two-part study, the performance of the vehicle is assessed. In particular, the key features of the optimal reference trajectories and controls are provided. The results of this study identify that as greater weight is placed on minimizing the height of the bunt maneuver or as the maximum altitude constraint is raised, the time of the bunt maneuver decreases and the time of the problem solution increases. Also, the results of this study identify that as the allowable crossrange of the vehicle is reduced, the time and height of the bunt maneuver increases and the time of the problem solution decreases.

Nomenclature

a	=	Speed of Sound
C_A	=	Axial Force Aerodynamic Coefficient
C_N	=	Normal Force Aerodynamic Coefficient
C_Y	=	Side Force Aerodynamic Coefficient
g_0	=	Standard Acceleration Due to Gravity, $\mathrm{m{\cdot}s^{-2}}$
h	=	Altitude Over Flat Earth
M	=	Mach Number
q	=	Dynamic Pressure
S	=	Vehicle Reference Area
t	=	Time
T	=	Thrust
v	=	Speed
x	=	Downtrack Displacement
y	=	Crosstrack Displacement

*Ph.D. Student, Department of Mechanical and Aerospace Engineering. E-mail: dennism09@ufl.edu.
†Associate Professor, Department of Mechanical and Aerospace Engineering. Erich Farber Faculty Fellow and University Term Professor. E-mail: anilvrao@ufl.edu. Corresponding Author.

z	=	Down Displacement
α	=	Pitch Angle
β	=	Sideslip Angle
γ	=	Flight Path Angle
ψ	=	Azimuth Angle
ρ	=	Atmospheric Density

I. Introduction

Optimal control problems arise frequently in many engineering applications due to the need to optimize performance of a controlled dynamical system. In general, optimal control problems do not have analytic solutions and, thus, must be solved numerically. Numerical methods for optimal control fall into two broad categories: indirect methods and direct methods. In an indirect method, the first-order variational optimality conditions are derived, and the optimal control problem is converted to a Hamiltonian boundary-value problem (HBVP). The HBVP is then solved numerically using a differential-algebraic equation solver. In a direct method, the state and control are approximated, and the optimal control problem is transcribed into a finite-dimensional nonlinear programming problem[1] (NLP). The NLP is then solved numerically using well developed software for solving NLPs.[2–4] Even in cases where an accurate approximation to the solution of an optimal control problem can be computed, disturbances in the actual system along with measurement errors lead to suboptimal performance and constraint violations in the actual system. If the difference between the motion of the reference system and that of the actual system is large, it may be necessary to re-solve the optimal control problem (that is, perform an optimal midcourse correction) in real-time based on the current state of the actual system. When re-solving the optimal control problem is necessary, it is desirable that the re-optimized solution be obtained sufficiently quickly so that this new solution can be implemented in the actual system. Because most optimal control problems must be solved numerically, in order to realize real-time optimal control in a constrained nonlinear dynamical system, it is necessary to develop computational methods.

A problem of current interest within the optimal control community is the optimal trajectory generation and guidance of air-to-surface missiles where the goal is to minimize the time required to reach a target from an initial state while performing a rapid maneuver toward the end of flight to attain the target condition. This research focuses on minimum-time trajectory and control generation for a low-altitude skid-to-turn air-to-surface missile. A particular problem that falls within the aforemetioned application realm are air-to-surface missiles where the goal is to minimize the time required to reach a target from an initial state. The problem of interest is one where the vehicle starts in a level flight configuration and is guided to terminal constraints on the position and velocity of the vehicle while being subject to additional altitude and crosstrack constraints during flight. The approach used in this paper is to employ the recently developed class of direct *Gaussian quadrature orthogonal collocation methods*.[5–19] In particular, the hp–adaptive Gaussian quadrature collocation approach is employed where it is possible to design a mesh that has the potential to provide equivalent or greater accuracy using a significantly smaller mesh than would be required using a traditional fixed-order collocation method. As a result, the computational efficiency of an hp method is potentially much greater when compared to that of a fixed-order method.

Previous work on trajectory optimization of air-to-surface missiles includes Refs. 20–22. Specifically, Ref. 20 studied the problem of trajectory optimization of a skid-to-turn air-to-surface missile with seeker angle constraints using a direct shooting method. Ref. 21 studied a problem similar to that of Ref. 20 using a bank-to-turn vehicle. Finally, Ref. 22 studied the problem of trajectory regulation using a linear quadratic follower approach to calculate a closed-loop in-flight control. In addition, Ref. 22 employed a preview term in order to predict the future trajectory from the current state. The approaches developed in Refs. 20–22 employed a shooting method for trajectory optimization and tracked the computed reference trajectory using a neighboring optimal control approach.[23]

Different from the research described in Refs. 20–22, in this paper, the problem of performance optimization of a skid-to-turn air-to-surface missile is investigated using a Legendre-Gauss-Radau collocation method.[6–14] The research described in this paper is the first part of a two-part sequence on trajectory optimization and guidance of a skid-to-turn vehicle. The trajectory optimization problem is posed as a two-phase optimal control problem using a weighted objective function. The objective function to be min-

imized is a combination of the first and second phases' terminal times and a penalty used to reduce the overall height and duration of the bunt maneuver. Because it is important that the maneuver to the target occur as late in the trajectory as possible with minimal height above a preselected altitude constraint, the objective function contains two terms: one term that minimizes the time of the maneuver and the overall time of the solution and one weighted penalty term that minimizes the overall height of the bunt maneuver. Furthermore, state constraints are imposed on the maximum altitude and the crossrange capability of the vehicle during the first phase of the maneuver. The altitude constraint ensures that the vehicle remains at a sufficiently low altitude until the terminal maneuver to the target is required, while the crossrange constraint ensures that the vehicle does not execute the terminal maneuver until necessary. Solutions are obtained as a function of the cost function's second term weight, the maximum allowable altitude, and the maximum allowable crossrange to examine the effect on the bunt maneuver.

This paper is organized as follows. Section II provides the equations of motion, vehicle model, and vehicle constraints. Section III provides a description of the optimal control problem. Section IV provides computational results obtained from solving the optimal control problem using various weighting factors, maximum allowable altitudes in phase one, and allowable crosstracks in phase one. Finally, Section V provides conclusions on this research.

II. Vehicle Model and Constraints

The goal of this research is to characterize the performance of a low-altitude skid-to-turn vehicle subject to constraints on altitude and crossrange. The problem under consideration is to perform a maneuver from an initial state to a target state such that the vehicle spends as much time as possible in near-steady and near-level flight while the time required to perform the bunt maneuver is as small as possible. In order to accomplish this combination of objectives, the flight of the vehicle is divided into two phases. In the first phase, the vehicle is subject to the aforementioned altitude and crossrange constraints. These constraints are removed in the second phase in order to enable the vehicle to attain the required terminal boundary conditions by performing a bunt maneuver. This section is divided into two parts. Section A provides the equations of motion and the vehicle model, while Section B provides the constraints imposed on the vehicle during flight.

A. Equations of Motion

Consider a vehicle modeled as a point mass in flight over a flat Earth subject to the forces of thrust, drag, lift, and gravity. The three degree-of-freedom equations of motion for the vehicle are given as

$$\begin{aligned}
\dot{x} &= v\cos\gamma\cos\psi, \\
\dot{y} &= v\cos\gamma\sin\psi, \\
\dot{z} &= -v\sin\gamma, \\
m\dot{v} &= (T-A)\cos\alpha\cos\beta - Y\sin\beta - N\sin\alpha\cos\beta - mg\sin\gamma, \\
mv\dot{\psi}\cos\gamma &= (T-A)\cos\alpha\sin\beta + Y\cos\beta - N\sin\alpha\sin\beta, \\
mv\dot{\gamma} &= (T-A)\sin\alpha + N\cos\alpha - mg\cos\gamma,
\end{aligned} \tag{1}$$

where x, y, and z are the displacements in the downtrack, crosstrack, and down directions, γ is the flight path angle (measured from the horizontal plane), ψ is the azimuth angle (measured clockwise from the downtrack direction), β is the sideslip angle, and α is the pitch angle. During flight, the vehicle is subject to the forces of gravity, mg, thrust, T (where T is the magnitude of the thrust), and aerodynamic axial, normal, and side forces, A, N, and Y, respectively. The three components A, N, and Y of the aerodynamic force are given, respectively, as

$$\begin{aligned}
A &= qSC_A, \\
N &= qSC_N, \\
Y &= qSC_Y,
\end{aligned} \tag{2}$$

where $q = \rho v^2/2$ is the dynamic pressure, ρ is the atmospheric density, S is the vehicle reference area, and C_A, C_N, and C_Y are the coefficients of axial force, normal force, and side force, respectively. The

aerodynamic force coefficients are obtained as

$$\begin{aligned} C_A &= C_A^b + C_A^w + C_A^t, \\ C_N &= C_N^w + C_N^t + C_N^b + C_N^m + C_N^{de}, \\ C_Y &= C_Y^w + C_Y^t + C_Y^b + C_Y^m + C_Y^{dr}, \end{aligned} \tag{3}$$

where

$$\begin{aligned} C_A^w &= \tfrac{1}{\pi r_w}\left([C_N^w]^2 + [C_Y^w]^2\right), \\ C_A^t &= \tfrac{1}{\pi r_t}\left(\left[C_N^t + C_N^{de}\right]^2 + \left[C_Y^t + C_Y^{dr}\right]^2\right), \end{aligned} \tag{4}$$

and

$$\begin{aligned} &C_N^w = C_N^{wa}\alpha/M, && C_N^t = C_N^{ta}\alpha/M, \\ &C_N^b = C_N^{ba}\alpha^2, && C_N^n = C_N^{na}\alpha, \\ &C_Y^w = -C_N^{wa}\beta/M, && C_Y^t = -C_N^{ta}\beta/M, \\ &C_Y^b = -C_N^{ba}\beta^2, && C_Y^n = -C_N^{na}\beta, \\ &C_M^w = r_1 C_N^w, && C_M^t = r_2 C_N^t, \\ &C_M^b = r_3 C_N^b, && C_M^n = r_4 C_N^n, \\ &C_P^w = r_1 C_Y^w, && C_P^t = r_2 C_Y^t, \\ &C_P^b = r_3 C_Y^b, && C_P^n = r_4 C_Y^n, \\ &C_M^0 = C_M^w + C_M^t + C_M^b + C_M^n, && C_P^0 = C_P^w + C_P^t + C_P^b + C_P^n, \\ &C_Y^{dr} = -C_P^0/r_2, && C_N^{de} = -C_M^0/r_2. \end{aligned} \tag{5}$$

The atmospheric density is given as

$$\rho(h) = \begin{cases} \rho_{10}\exp(-h/H_1) & , \quad 0 \leq h \leq h^\rho, \\ \rho_{20}\exp(-h/H_2) & , \quad h^\rho < h < \infty, \end{cases} \tag{6}$$

where $h = -z$. Next, the speed of sound given as

$$a(h) = \begin{cases} c_1 h + c_0 & , \quad 0 \leq h \leq h_1^a \\ d_0 & , \quad h_1^a < h < h_2^a \\ e_1 h + e_0 & , \quad h_2^a \leq h < \infty. \end{cases} \tag{7}$$

The Mach number is given as

$$M = \sqrt{\frac{v^2}{a^2} - 1}. \tag{8}$$

Finally, the coefficients corresponding to the aerodynamic model given in Eqs. (2)–(8) are given in Table 1.

B. Constraints

The problem considered consists of two phases, and the following constraints are imposed on the vehicle during flight in each of the two phases. In the first phase, the altitude and crosstrack are constrained in order to delay the time at which a bunt maneuver by the vehicle is completed in order to attain the target conditions. Thus, in the first phase, the altitude is constrained as

$$h_{\min}^{(1)} \leq h^{(1)} \leq h_{\max}^{(1)}, \tag{9}$$

and the crosstrack is constrained as

$$y_{\min}^{(1)} \leq y^{(1)} \leq y_{\max}^{(1)}. \tag{10}$$

Next, the components of the state and the components of the control are constrained to remain within the following limits during both phases of flight:

$$\begin{aligned} (x_{\min}, y_{\min}, z_{\min}, v_{\min}, \gamma_{\min}, \psi_{\min}) &\leq (x, y, z, v, \gamma, \psi) \leq (x_{\max}, y_{\max}, z_{\max}, v_{\max}, \gamma_{\max}, \psi_{\max}), \\ (\alpha_{\min}, \beta_{\min}, T_{\min}) &\leq (\alpha, \beta, T) \leq (\alpha_{\max}, \beta_{\max}, T_{\max}), \end{aligned} \tag{11}$$

Table 1: Vehicle Model Constants.

Quantity	Value
S	0.0730 m^2
r_w	2.0833
r_t	6.25
C_N^{wa}	61.1155
C_N^{ta}	20.3718
C_N^{ba}	36.3064
C_N^{na}	2
C_A^b	0.1522
g	9.81 $\mathrm{m} \cdot \mathrm{s}^{-2}$
m	453.2268 kg
r_1	-1.2
r_2	-9.5
r_3	-0.4966
r_4	8
ρ_{10}	1.2256 $\mathrm{kg} \cdot \mathrm{m}^{-3}$
ρ_{20}	1.7523 $\mathrm{kg} \cdot \mathrm{m}^{-3}$
H_1	9144 m
H_2	6705.6 m
c_0	340.2940 $\mathrm{m} \cdot \mathrm{s}^{-1}$
c_1	-0.004 s^{-1}
d_0	295.0464 $\mathrm{m} \cdot \mathrm{s}^{-1}$
e_0	281.9370 $\mathrm{m} \cdot \mathrm{s}^{-1}$
e_1	0.0007 s^{-1}
h^ρ	9144 m
h_1^a	11277.6 m
h_2^a	19507.2 m

where the minimum and maximum allowable values corresponding to the state and control components given in Eqs. (9)–(11) are given in Table 2. Furthermore, the Mach number is constrained

$$M_{\min} \leq M \leq M_{\max}, \tag{12}$$

where the values $(M_{\min}, M_{\max})$ are given in Table 2. In addition, the state and time at the terminus of the first phase are connected to the state and time at the start of the second phase through interior-point event constraints. The interior point event constraints are given as

$$\begin{aligned}
t_f^{(p)} - t_0^{(p+1)} &= 0, \\
x(t_f^{(p)}) - x(t_0^{(p+1)}) &= 0, \\
y(t_f^{(p)}) - y(t_0^{(p+1)}) &= 0, \\
z(t_f^{(p)}) - z(t_0^{(p+1)}) &= 0, \quad p \in [1]. \\
v(t_f^{(p)}) - v(t_0^{(p+1)}) &= 0, \\
\gamma(t_f^{(p)}) - \gamma(t_o^{(p+1)}) &= 0, \\
\psi(t_f^{(p)}) - \psi(t_0^{(p+1)}) &= 0,
\end{aligned} \tag{13}$$

Finally, the boundary conditions imposed on the vehicle at the start of the first phase and the terminus of the second phase are given as

$$\begin{array}{rclcrcl} x\left(t_0^{(1)}\right) & = & x_0 & , & x\left(t_f^{(2)}\right) & = & x_f, \\ y\left(t_0^{(1)}\right) & = & y_0 & , & y\left(t_f^{(2)}\right) & = & y_f, \\ z\left(t_0^{(1)}\right) & = & z_0 & , & z\left(t_f^{(2)}\right) & = & z_f, \\ v\left(t_0^{(1)}\right) & = & v_0 & , & v\left(t_f^{(2)}\right) & = & v_f, \\ \gamma\left(t_0^{(1)}\right) & = & \gamma_0 & , & \gamma\left(t_f^{(2)}\right) & = & \gamma_f \\ \psi\left(t_0^{(1)}\right) & = & \psi_0 & , & \psi\left(t_f^{(2)}\right) & = & \text{Free}, \end{array} \tag{14}$$

where the initial and terminal values of the state components are given in Table 2.

Table 2: Lower and upper limits on state bounds and path constraints along with boundary conditions on the state and control.

Quantity	Value
$(x_{\min}, x_{\max})$	$(0, 46000)$ m
$(y_{\min}, y_{\max})$	$(-77000, 77000)$ m
$(y^{(1)}_{\min}, y^{(1)}_{\max})$	$(-50000, 50000)$ m
$(z_{\min}, z_{\max})$	$(-15300, 0)$ m
$(h^{(1)}_{\min}, h^{(1)}_{\max})$	$(10, 170)$ m
$(v_{\min}, v_{\max})$	$(16, 1220)$ m/s
$(\gamma_{\min}, \gamma_{\max})$	$(-89, 89)$ deg
$(\psi_{\min}, \psi_{\max})$	$(-180, 180)$ deg
$(\alpha_{\min}, \alpha_{\max})$	$(-6, 6)$ deg
$(\beta_{\min}, \beta_{\max})$	$(-6, 6)$ deg
$(T_{\min}, T_{\max})$	$(2225, 8900)$ N
$(M_{\min}, M_{\max})$	$(2, 4.5)$
$t_0^{(1)}$	0 s
(x_0, x_f)	$(0, 30500)$ m
(y_0, y_f)	$(0, 6100)$ m
(z_0, z_f)	$(-31, 0)$ m
(v_0, v_f)	$(915, 915)$ m·s^{-1}
(γ_0, γ_f)	$(0, -85)$ deg
ψ_0	0 deg

III. Optimal Control Problem

Using the vehicle model and contraints given in Section II, the optimal control problem is stated as follows. Determine the state $(x(t), y(t), z(t), v(t), \gamma(t), \psi(t))$, control $(\alpha(t), \beta(t), T(t))$, and final time $(t_f^{(1)}, t_f^{(2)})$ in each phase that minimizes the objective function

$$J = t_f^{(2)}\left(t_f^{(2)} - t_f^{(1)}\right)^2 + W\int_{t_0^{(1)}}^{t_f^{(2)}} |h - h^{(1)}_{\max}|dt \tag{15}$$

subject to the dynamic constraints given in Eq. (1), the limits on the components of the state and control given in Eqs. (9)–(11), the path constraint given in Eq. (12), the interior point event constraints given in Eq. (13), and the boundary conditions given in Eq. (14). The objective function in Eq. (15) combines the

desire to shorten the duration of phases one and two while reducing the overall height and duration of the maneuver in phase two. Using an objective function of this form enables delaying the maneuver necessary to attain the target condition for as long as possible, thereby allowing the vehicle to move for as long as possible along a path where the altitude changes are reduced. The weighting factor, W, is used to penalize a solution that produces a higher and longer bunt maneuver in phase two.

IV. Results and Discussion

All results shown in this paper were obtained using the MATLAB® optimal control software $\mathbb{GPOPS}-\mathbb{II}$[24] with the nonlinear programming problem (NLP) solver *IPOPT*,[4] where *IPOPT* was employed in full Newton (second derivative) using the default NLP solver tolerance of $\epsilon_{\text{NLP}} = 10^{-7}$. Any necessary mesh refinement was performed using the mesh refinement method described in Ref. 14 using a minimum of three and maximum of fourteen allowable collocation points per interval and a mesh refinement relative-error accuracy tolerance of $\epsilon_{\text{mesh}} = 10^{-5}$. The initial mesh size of each phase is ten mesh intervals with five collocation points each. In order to employ *IPOPT* in full Newton mode, all required first and second derivatives were obtained using the algorithmic differentiation software *ADiGator*.[25] Finally, all computations shown in this section were on a 3.1 GHz Intel Core i7 MacBook Pro running Mac OS-X version 10.12.6 (Sierra) with 16GB 1867MHz DDR3 RAM and MATLAB® Version R2016a (build 9.0.0.341360).

The results in this section are divided into four sections. Section A is the solution to the optimal control problem in Section III for one maximum altitude constraint, $h^{(1)}_{\max} = 170$ m, in the first phase using the objective function in Eq. (15) with a weighting factor of $W = 0.5$. This is highlighted to show how the state and control in each phase behave. Section B is the solutions to the optimal control problem for a set of weighting factors, $W = (0, 0.25, 0.50, 0.75, 1)$, using the objective function in Eq. (15) and one set altitude constraint, $h^{(1)}_{\max} = 170$ m. Section C is the solutions to the optimal control problem for a set of maximum altitude constraints, $h^{(1)}_{\max} = (50, 90, 130, 170, 210\,\text{m})$, with a weighting factor of $W = 0.5$ using the objective function in Eq. (15). The altitude constraint is set such that the vehicle can maneuver in the h-direction from $h^{(1)}_{\min} = 10$ m to $h^{(1)}_{\max}$ in phase one. Section D is the solutions to the optimal control problem for a set of minimum and maximum crosstrack constraints $\left[(y^{(1)}_{\min} = -10, -20, -30, -40, -50\,\text{km}), (y^{(1)}_{\max} = 10, 20, 30, 40, 50\,\text{km})\right]$ using one set altitude constraint, $h^{(1)}_{\max} = 170$ m, with a weighting factor of $W = 0.5$ in the objective function of Eq. (15). The crosstrack constraint is set such that the vehicle can maneuver in the y-direction from $y^{(1)}_{\min}$ to $y^{(1)}_{\max}$ in phase one.

A. Initial Problem Solution

The state and control solution to the optimal control problem described in Section III with a weighting factor of $W = 0.5$ is shown in Figs. 1–3. The path constraint over the solution set is shown in Fig. 4. Figure 1a shows the three-dimensional trajectory to the optimal control problem. It can be seen in Fig. 2 that the altitude, $h = -z$, in the first phase consists of an initial ascent to a constant altitude that is equivalent to the state component's constraint, $h^{(1)}_{\max} = 170$ m. In addition, the first phase terminates with a slight decrease in altitude followed by an increase in altitude as the vehicle prepares to execute a bunt maneuver. In the second phase, as seen in Fig. 1, the bunt maneuver starts as the vehicle climbs to its maximum altitude and then descends in order to meet the terminal constraints. The total time of the two phases is 119.89 s, and the vehicle spends 46.85 s in phase two. It is seen from the solution in Fig. 1c that the vehicle never attains the maximum allowable speed, $v_{\max} = 1220\ \text{m} \cdot \text{s}^{-1}$; however, the thrust is at its maximum, $T_{\max} = 8900$ N, for the entire solution as seen in Fig. 3c. Next, Fig. 4 shows the Mach number as a function of time. It is seen that the Mach number path constraint, given in Eq. (12), is never active.

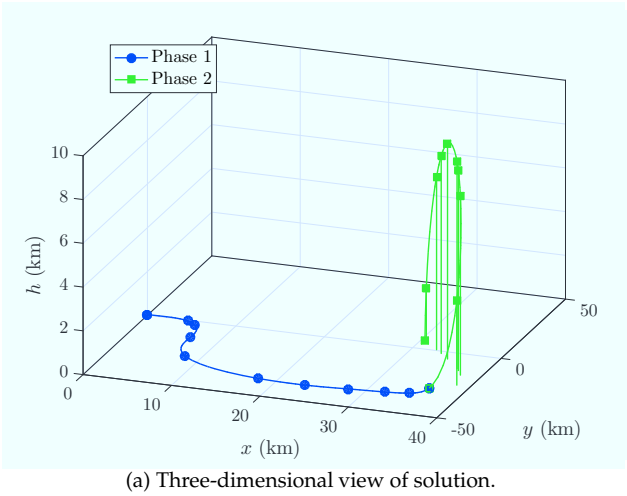

(a) Three-dimensional view of solution.

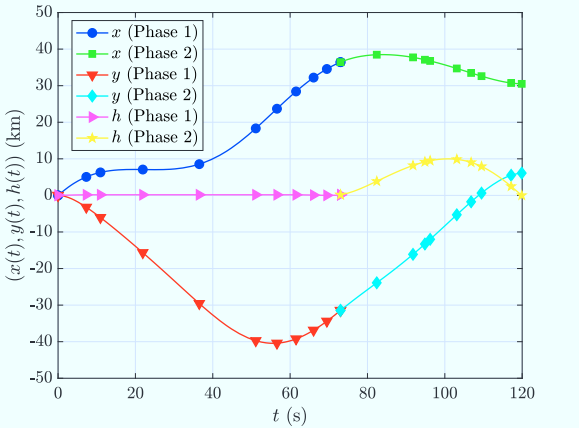

(b) Downtrack, $x(t)$, crosstrack, $y(t)$, and altitude, $h(t)$, vs. t.

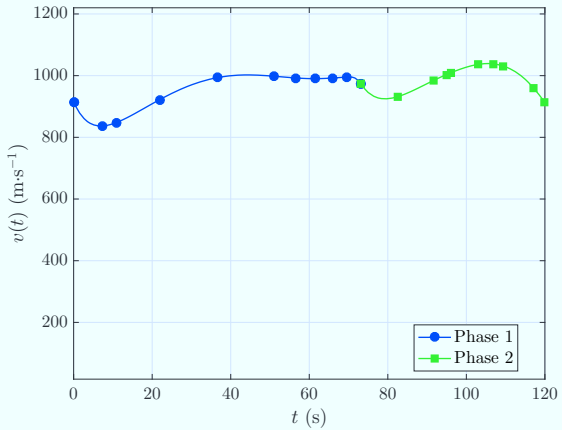

(c) Speed, $v(t)$, vs. t.

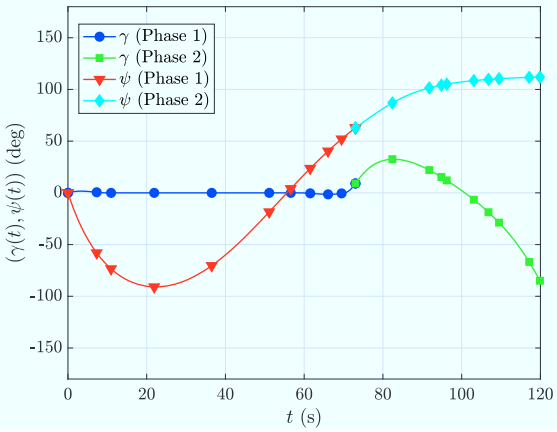

(d) Flight path angle, $\gamma(t)$, and azimuth angle, $\psi(t)$, vs. t.

Figure 1: State solution, $(x(t), y(t), h(t), v(t), \gamma(t), \psi(t))$, vs. t of the optimal control problem described in Section III with a weighting factor of $W = 0.5$ and an altitude constraint of $h_{\max}^{(1)} = 170$ m.

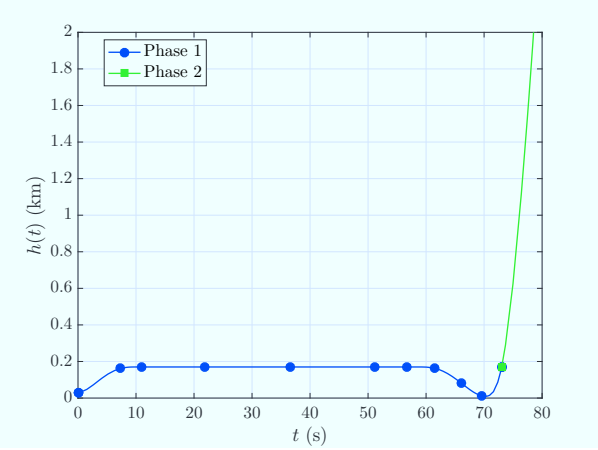

Figure 2: Phase one of altitude solution, $h(t)$, vs. t of the optimal control problem described in Section III with a weighting factor of $W = 0.5$ and an altitude constraint of $h_{\max}^{(1)} = 170$ m.

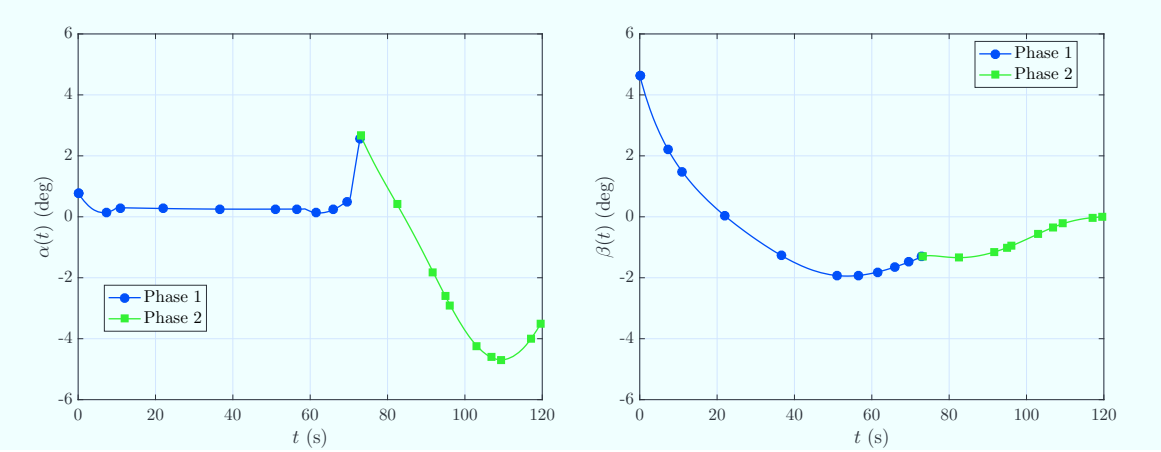

(a) Pitch angle, $\alpha(t)$, vs. t.

(b) Side slip angle, $\beta(t)$, vs. t.

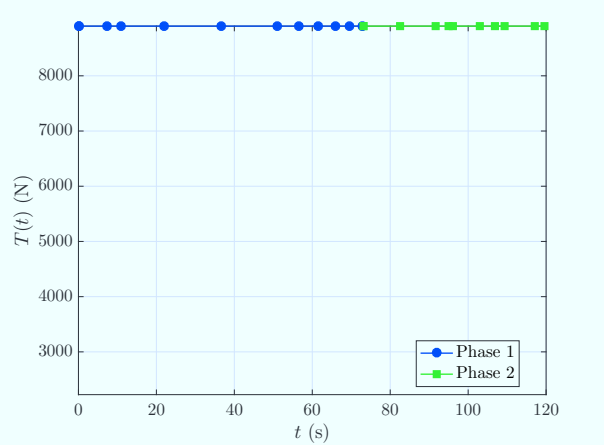

(c) Thrust magnitude, $T(t)$, vs. t.

Figure 3: Control solution, $(\alpha(t), \beta(t), T(t))$, vs. t of the optimal control problem described in Section III with a weighting factor of $W = 0.5$ and an altitude constraint of $h_{\max}^{(1)} = 170$ m.

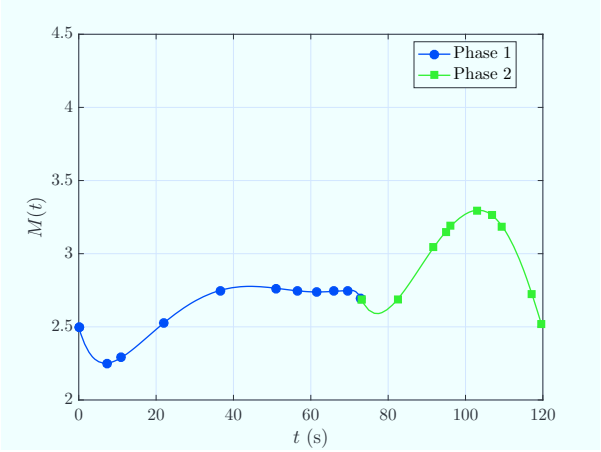

Figure 4: Mach number, $M(t)$, vs. t on solution to the optimal control problem described in Section III with a weighting factor of $W = 0.5$ and an altitude constraint of $h_{\max}^{(1)} = 170$ m.

B. Study 1: Varying Weights in Objective Function

The optimal control problem described in Section III is solved using the objective function in Eq. (15) with a set of weighting factors, $W = (0, 0.25, 0.50, 0.75, 1)$, and an altitude constraint in phase one, $h_{\max}^{(1)} = 170$ m. Figs. 5–8 show the solutions to the optimal control problem for the range of weighting factors. It is seen from Fig. 6 and Table 3 that the overall time of the solution increases while the time and height of the bunt maneuver in phase two decreases as the weighting factor increases.

It is important to note that the solution when $W = 0$ is significantly different than the solutions when $W \neq 0$. The objective function in Eq. (15) consists of two terms: one a function of time and one a function of altitude. When $W = 0$, the objective function is reduced to one term, which is only a function of time. Because the objective function is reduced and the cost of the solution is not impacted by the altitude of the vehicle, the solution to the optimal control problem takes a different form where the bunt maneuver is much longer and higher than the solutions that have a nonzero W. Figure 7 magnifies the altitude solution in phase one, showing that the vehicle increases altitude until it reaches the altitude constraint, $h_{\max}^{(1)} = 170$ m, for all solutions where the objective function has the second penalty term. When $W = 0$, the vehicle does not spend much time in phase one; therefore, the vehicle does not maintain level flight at the maximum altitude constraint for any period of time. To reduce the time and height of the bunt maneuver when the objective function has a nonzero weighting factor, $W \neq 0$, it can be seen in Fig. 6b that the vehicle has a greater crossrange in phase one of the solution. When $W = 0$, the bunt maneuver occurs over a much smaller downtrack and crosstrack regime; the vehicle has a more direct trajectory between the initial and terminal conditions in the downtrack-crosstrack plane. Table 3 shows the time of the bunt maneuver in phase two, the total time of the solution, the maximum height of the bunt maneuver in phase two, and the objective value of each solution to the optimal control problem.

Given the results in Table 3, it is necessary to have the second term in the objective function in Eq. (15) to ensure the vehicle remains in level, steady flight for an extended period of time before executing the maneuver in phase two. Also, as seen in Figs. 6e and 8a, the flight path angle and angle of attack of each solution are most influenced by the variation in the weighting factor. More specifically, the flight path angle and angle of attack profiles are shifted in time as a result of the second phases starting at a later time. Also, the flight path angle, azimuth angle, and sideslip angles all have similar solutions, with the solutions associated with $W = 0$ being earlier and longer as the bunt maneuver occurs earlier and longer in comparison to the other solutions. The speed and pitch angle, as seen in Figs. 6d and 8a, are most affected by the addition of the second term in the objective function. The Mach number path constraint is never active as seen in Fig. 9 for solutions where $W \neq 0$. The lower Mach number path constraint is active on two arcs when $W = 0$, as the vehicle is ascending towards its maximum altitude and as the vehicle is at its maximum altitude. The thrust, as seen in Fig. 8c, is still at its maximum throughout the problem, regardless of the weighting factor.

Table 3: Time of bunt maneuver, $(t_f^{(2)} - t_f^{(1)})$, time of total solution, $t_f^{(2)}$, maximum height of vehicle in phase two, $h_{\max}^{(2)}$, and objective value, J, obtained from the optimal control problem solutions evaluated at the various weighting factors, $W = (0, 0.25, 0.50, 0.75, 1)$.

Weighting factor, W	$(t_f^{(2)} - t_f^{(1)})$, s	$t_f^{(2)}$, s	$h_{\max}^{(2)}$, km	$J \times 10^5$
0	60.92	62.46	13.06	2.32
0.25	48.04	111.87	10.18	3.31
0.50	46.85	119.89	9.99	4.02
0.75	46.15	125.91	9.88	4.71
1	45.67	130.96	9.80	5.37

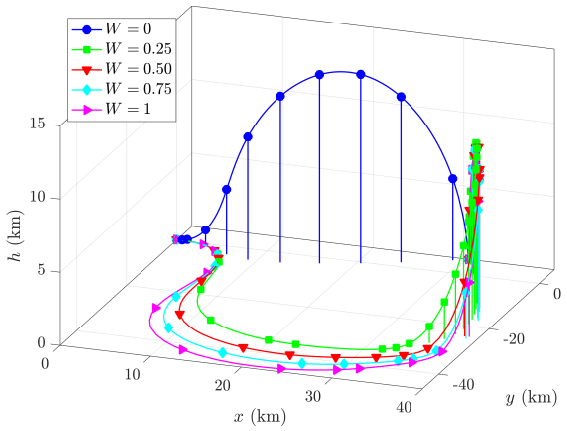

Figure 5: Three-dimensional trajectories obtained from the solution of the optimal control problem described in Section III for a range of weights in the cost function of Eq. (15) and an altitude constraint of $h^{(1)}_{\max} = 170$ m.

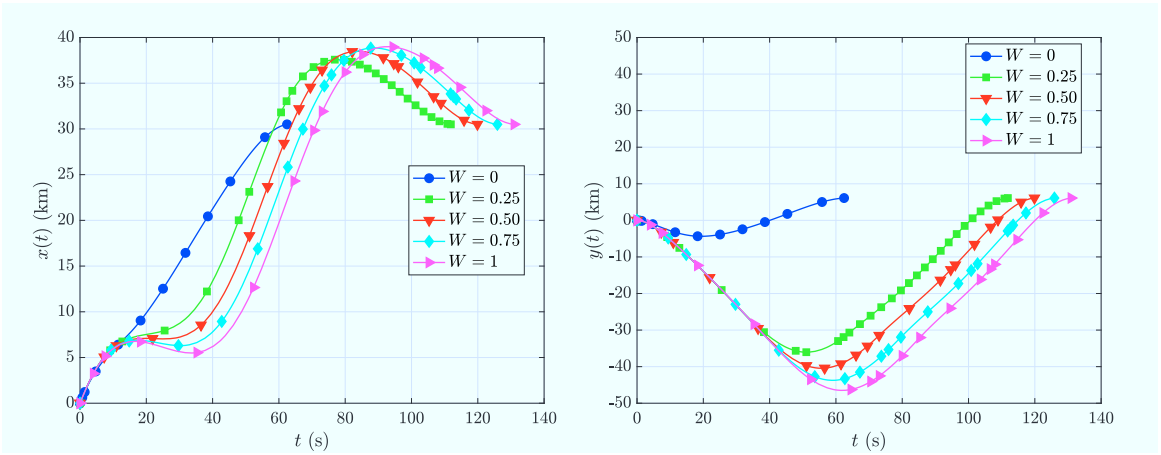

(a) Downtrack, $x(t)$, vs. t.

(b) Crosstrack, $y(t)$, vs. t.

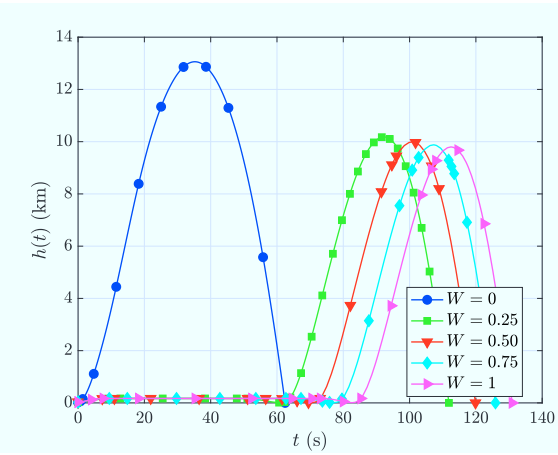

(c) Altitude, $h(t)$, vs. t.

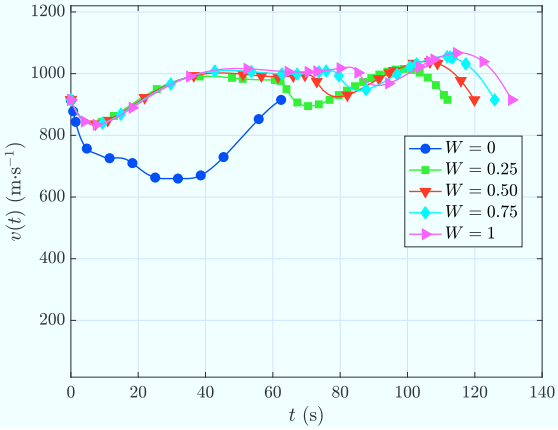

(d) Speed, $v(t)$, vs. t.

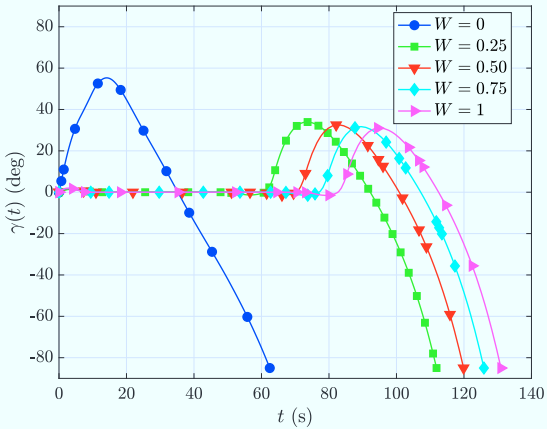

(e) Flight path angle, $\gamma(t)$, vs. t.

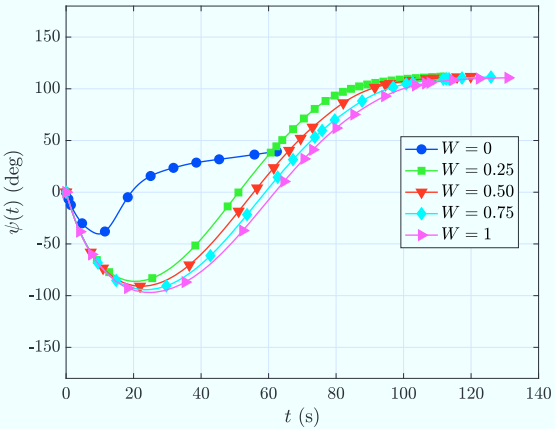

(f) Azimuth angle, $\psi(t)$, vs. t.

Figure 6: State solution, $(x(t), y(t), h(t), v(t), \gamma(t), \psi(t))$, vs. t of the optimal control problem described in Section III for a range of allowable weights in the cost function of Eq. (15) and an altitude constraint of $h^{(1)}_{\max} = 170$ m.

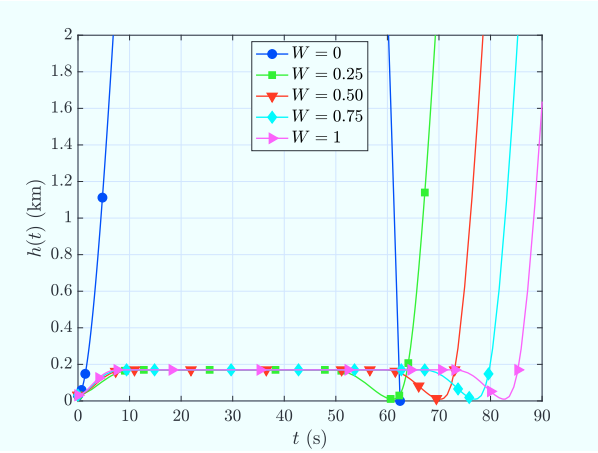

Figure 7: Altitude, $h(t)$, vs. t on solution to the optimal control problem described in Section III for a range of allowable weights in the cost function of Eq. (15) in phase one.

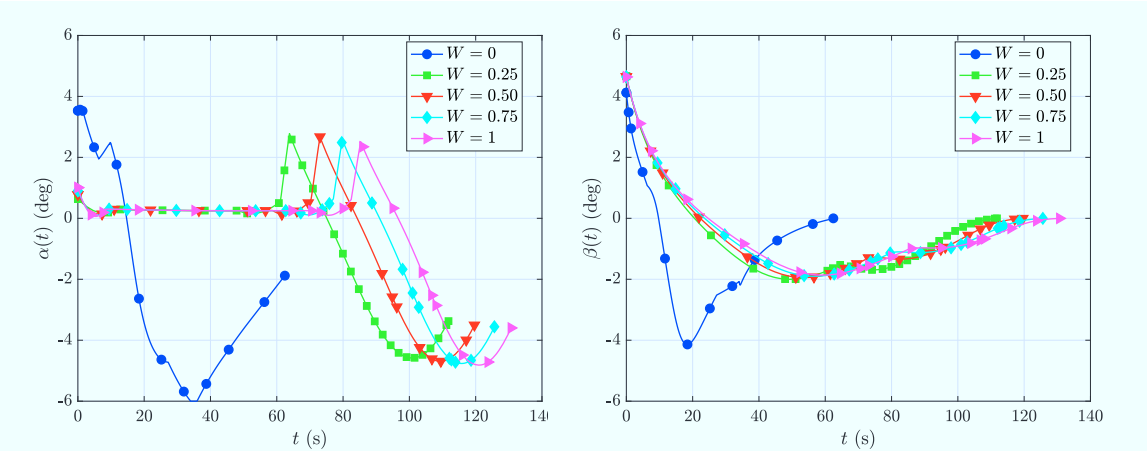

(a) Pitch angle, $\alpha(t)$, vs. t.

(b) Slip angle angle, $\beta(t)$, vs. t.

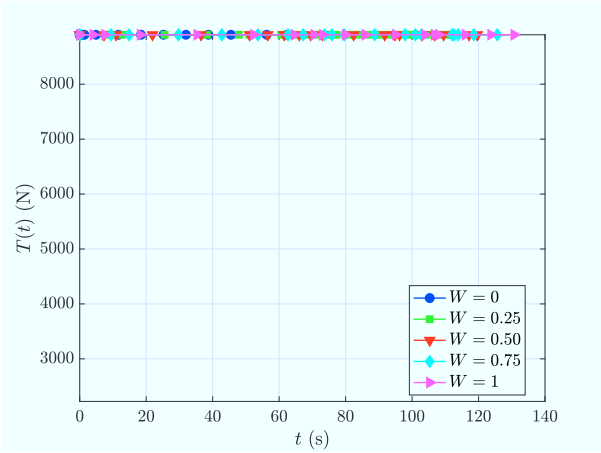

(c) Thrust magnitude, $T(t)$, vs. t.

Figure 8: Control solution, $(\alpha(t), \beta(t), T(t))$, vs. t of the optimal control problem described in Section III for a range of weights in the cost function of Eq. (15) and an altitude constraint of $h^{(1)}_{\max} = 170$ m.

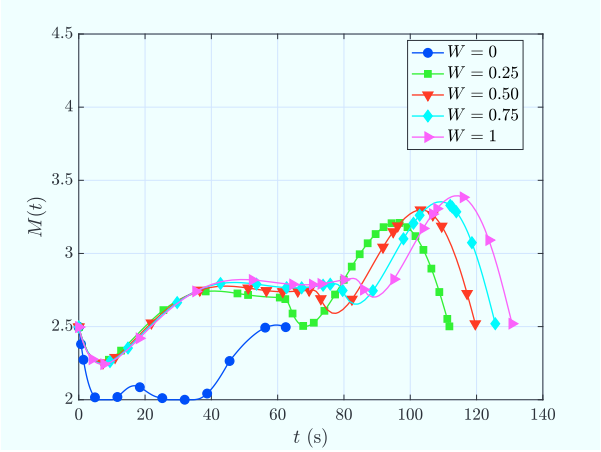

Figure 9: Mach number, $M(t)$, vs. t on solution to the optimal control problem described in Section III for a range of weights in the cost function of Eq. (15) and an altitude constraint of $h^{(1)}_{\max} = 170$ m.

C. Study 2: Varying Maximum Altitude Constraints

The optimal control problem described in Section III is solved with a set of altitude constraints in phase one, $h^{(1)}_{\max} = (50, 90, 130, 170, 210)$ m, using the objective function in Eq. (15) with a weighting factor of $W = 0.5$. Figures 10–13 show the solutions to the optimal control problem for the range of altitude constraints. It can be seen that the change in maximum altitude allowed during phase one of the problem does not create a significant change in the solutions. Figure 12 magnifies the altitude in phase one and shows that the vehicle increases altitude until it reaches the maximum altitude constraint for the first phase. At the end of phase one for each solution, there is a decrease in altitude as the vehicle prepares to begin the bunt maneuver. It is also noted that although the maximum allowable altitudes in phase one are different, the time at which the bunt maneuvers are initially executed are very similar. As the solutions being nearly identical, the Mach number path constraint is also never active, as seen in Fig. 14, and the thrust is at its maximum throughout the entire solution, as seen in Fig. 13c. Table 4 shows the time of the bunt maneuver in phase two, the total time of the solution, the maximum height of the bunt maneuver in phase two, and the objective value of each solution to the optimal control problem.

Table 4: Time of bunt maneuver, $(t^{(2)}_f - t^{(1)}_f)$, time of total solution, $t^{(2)}_f$, maximum height of vehicle in phase two, $h^{(2)}_{\max}$, and objective value, J, obtained from the optimal control problem solutions evaluated at the various maximum altitudes, $h^{(1)}_{\max} = (50, 90, 130, 210, 250)$ m.

$h^{(1)}_{\max}$, m	$(t^{(2)}_f - t^{(1)}_f)$, s	$t^{(2)}_f$, s	$h^{(2)}_{\max}$, km	$J \times 10^5$
50	48.05	119.00	10.01	4.18
90	47.55	119.45	10.01	4.12
130	47.17	119.76	10.00	4.07
170	46.85	119.89	9.99	4.02
210	46.54	120.24	9.98	3.98

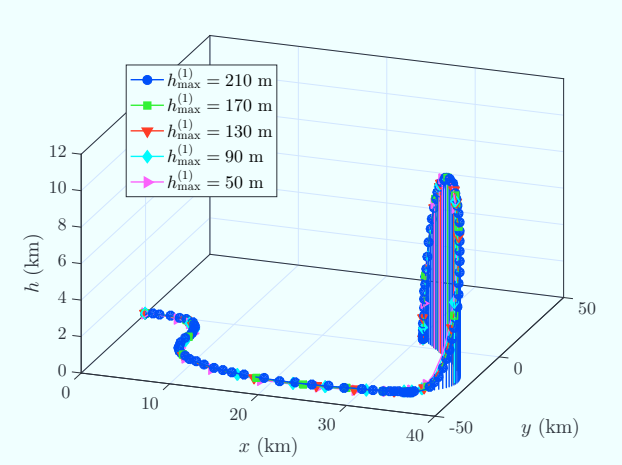

Figure 10: Three-dimensional trajectories obtained from the solution of the optimal control problem described in Section III for a range of maximum allowable altitudes in the first phase with the cost function in Eq. (15) and a weighting factor $W = 0.5$.

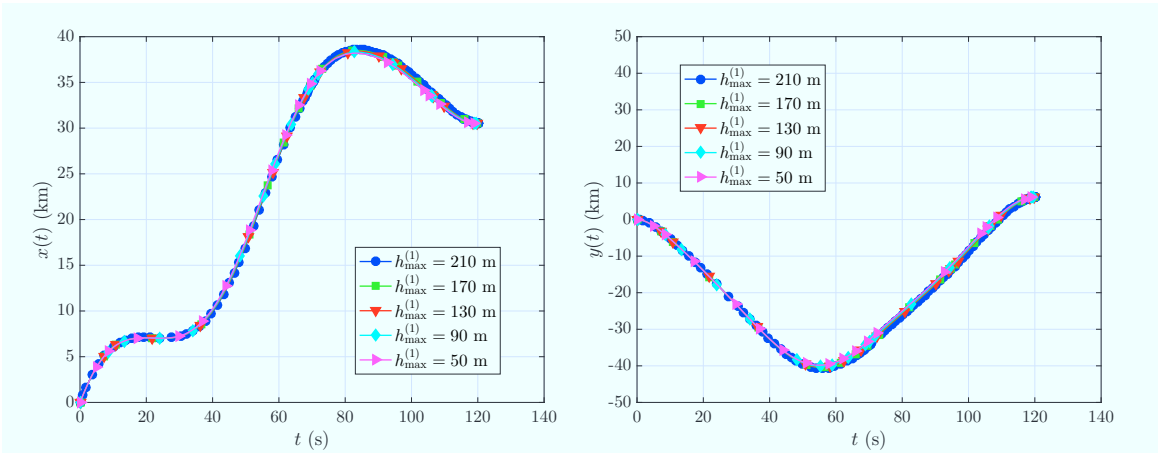

(a) Downtrack, $x(t)$, vs. t.

(b) Crosstrack, $y(t)$, vs. t.

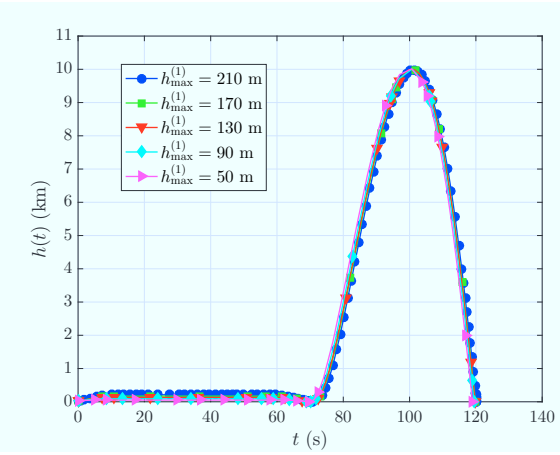

(c) Altitude, $h(t)$, vs. t.

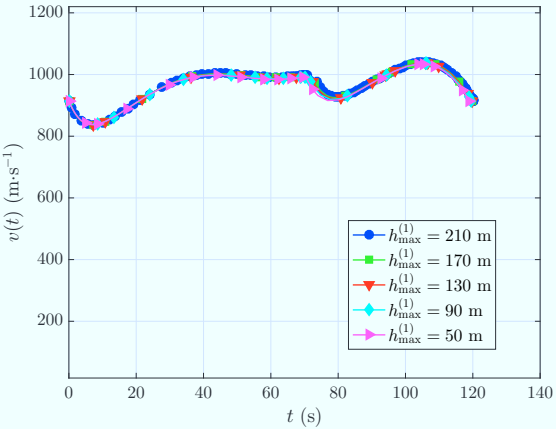

(d) Speed, $v(t)$, vs. t.

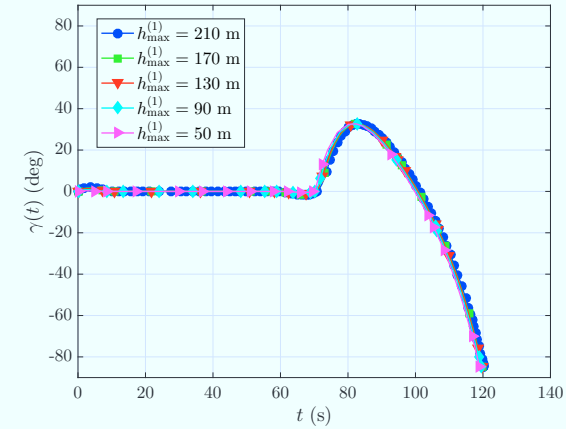

(e) Flight path angle, $\gamma(t)$, vs. t.

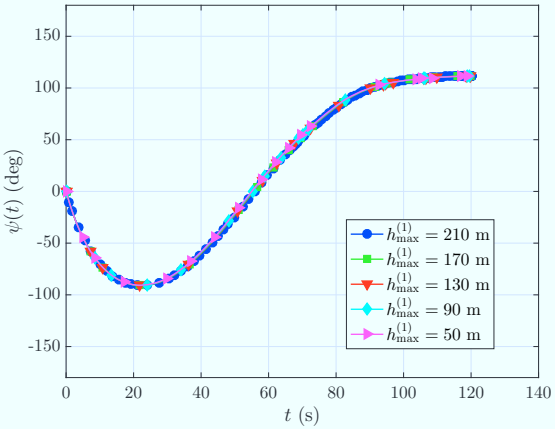

(f) Azimuth angle, $\psi(t)$, vs. t.

Figure 11: State solution, $(x(t), y(t), h(t), v(t), \gamma(t), \psi(t))$, vs. t of the optimal control problem described in Section III for a range of maximum allowable altitudes in the first phase with the cost function in Eq. (15) and a weighting factor $W = 0.5$.

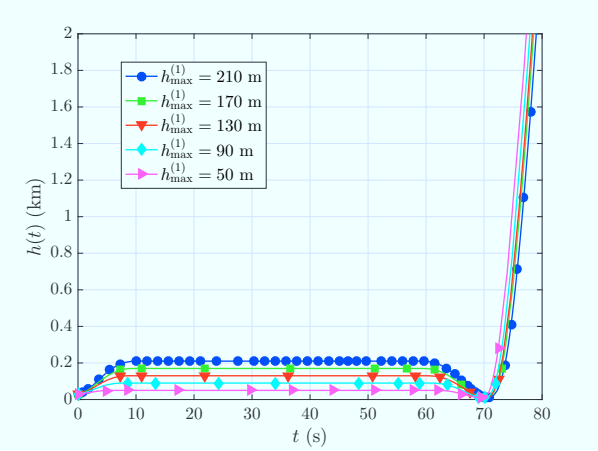

Figure 12: Altitude, $h(t)$, vs. t on solution to the optimal control problem described in Section III for a range of maximum allowable altitudes in the first phase with the cost function in Eq. (15) and a weighting factor $W = 0.5$.

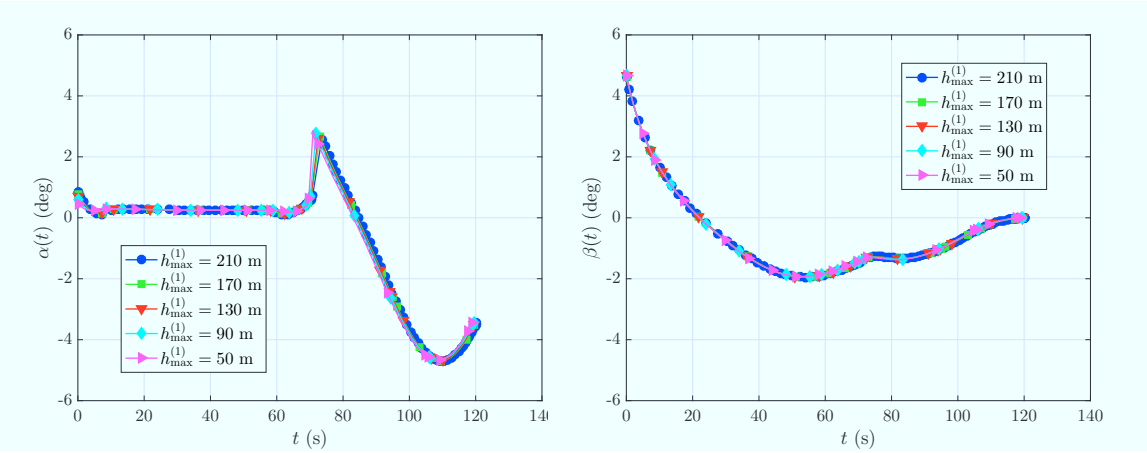

(a) Pitch angle, $\alpha(t)$, vs. t.

(b) Slip angle angle, $\beta(t)$, vs. t.

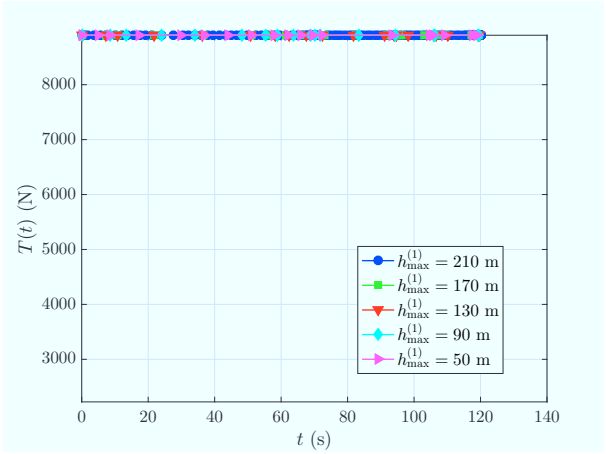

(c) Thrust magnitude, $T(t)$, vs. t.

Figure 13: Control solution, $(\alpha(t), \beta(t), T(t))$, vs. t of the optimal control problem described in Section III for a range of maximum allowable altitudes in the first phase with the cost function in Eq. (15) and a weighting factor $W = 0.5$.

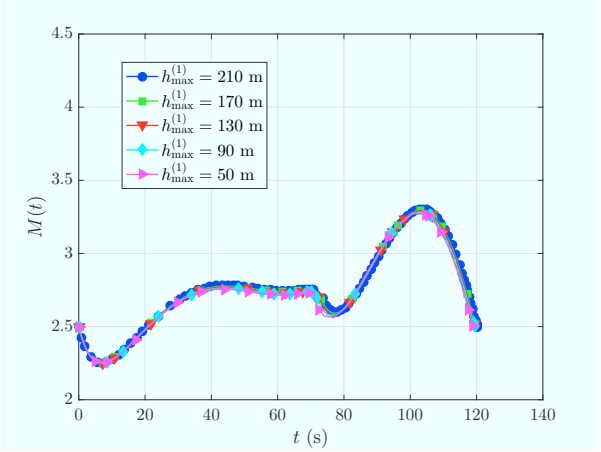

Figure 14: Mach number, $M(t)$, vs. t on solution to the optimal control problem described in Section III for a range of maximum allowable altitudes in the first phase with the cost function in Eq. (15) and a weighting factor $W = 0.5$.

D. Study 3: Varying Maximum Crossrange Constraints

The optimal control problem described in Section III is solved with a set of crosstrack ranges in phase one, $\left[y^{(1)}_{\min} = (-10, -20, -30, -40, -50)\text{ km}, y^{(1)}_{\max} = (10, 20, 30, 40, 50)\text{ km}\right]$, a constant altitude constraint, $h^{(1)}_{\max} = 170$ m, and a weighting factor of $W = 0.5$, using the objective function in Eq. (15). Figures 15–18 show the solutions to the optimal control problem for the range of crosstrack constraints. Figure 15 shows the three-dimensional trajectories to the optimal control problem for the range of minimum and maximum allowable crossranges in the first phase. As the crosstrack range decreases, phase two begins sooner which results in a higher maximum bunt altitude and a longer bunt maneuver, as seen in Fig. 16 and Table 5. Also, as seen in Figs. 16a–16b, the greater restriction in crossrange produces a solution where the vehicle moves over a small regime between the initial and terminal conditions in the downrange-crossrange plane. As the crosstrack range is relaxed, the solution deviates from this small regime between the initial and terminal conditions. This can especially be seen in the solutions where $y^{(1)}_{\min} \leq -30$ km. In these solutions, the vehicle moves past the target in the downrange direction and doubles back in phase two to meet the terminal conditions (as seen in Figs. 15 and 16a). As a result, as the crossrange constraints are relaxed, the overall time of the solution increases while the time and height of the bunt maneuver in phase two decreases, as seen in Table 5. It is worth noting that the solution to the optimal control problem in Section A is the solution to this problem with the most relaxed crosstrack range. As a result, the solution to the optimal control problem does not change as the crossrange constraints are relaxed past $y^{(1)}_{\min} \leq -50$ km and $y^{(1)}_{\max} \geq 50$ km. Figure 17 magnifies the altitude in phase one, showing that the vehicle increases altitude until it reaches the altitude constraint in phase one, $h^{(1)}_{\max} = 170$ m. At the end of phase one for each solution, there is a decrease in altitude as the vehicle prepares to begin the bunt maneuver. Also, as a result, the flight path angle and angle of attack profiles are shifted in time as a result of the second phases starting at an earlier time, as seen in Figs. 16e and 18a. The Mach number path constraint is almost active, as seen in Fig. 19, when the crosstrack is at its smallest range; however, the Mach number path constraint is never active throughout the other problem solutions. The thrust is at its maximum for the entire solution as seen in Fig. 18c.

Table 5: Time of bunt maneuver, $(t_f^{(2)} - t_f^{(1)})$, time of total solution, $t_f^{(2)}$, maximum height of vehicle in phase two, $h_{\max}^{(2)}$, and objective value, J, obtained from the optimal control problem solutions evaluated at the various crossranges $\left[y_{\min}^{(1)} = (-10, -20, -30, -40, -50)\,\text{km}, y_{\max}^{(1)} = (10, 20, 30, 40, 50)\,\text{km}\right]$.

$y_{\min}^{(1)}$, km	$y_{\max}^{(1)}$, km	$(t_f^{(2)} - t_f^{(1)})$, s	$t_f^{(2)}$, s	$h_{\max}^{(2)}$, km	$J \times 10^5$
-10	10	59.55	75.14	11.96	4.84
-20	20	55.65	84.08	11.22	4.50
-30	30	50.46	100.44	10.48	4.14
-40	40	46.96	119.13	10.01	4.02
-50	50	46.85	119.89	9.99	4.02

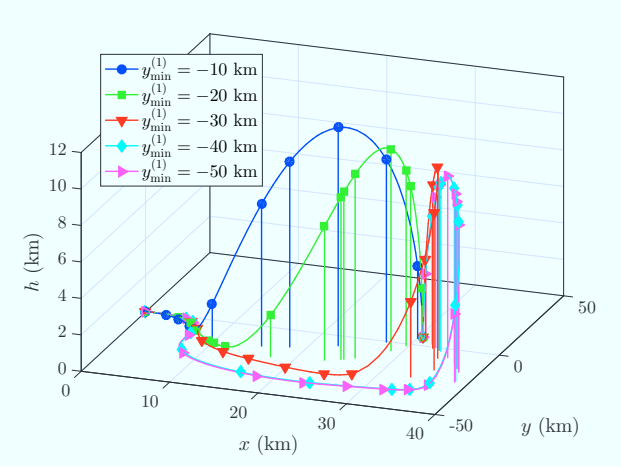

Figure 15: Three-dimensional trajectories obtained from the solution of the optimal control problem described in Section III for a range of minimum and maximum allowable crossrange in the first phase with the cost function in Eq. (15) with an altitude constraint of $h_{\max}^{(1)} = 170$ m and a weighting factor of $W = 0.5$.

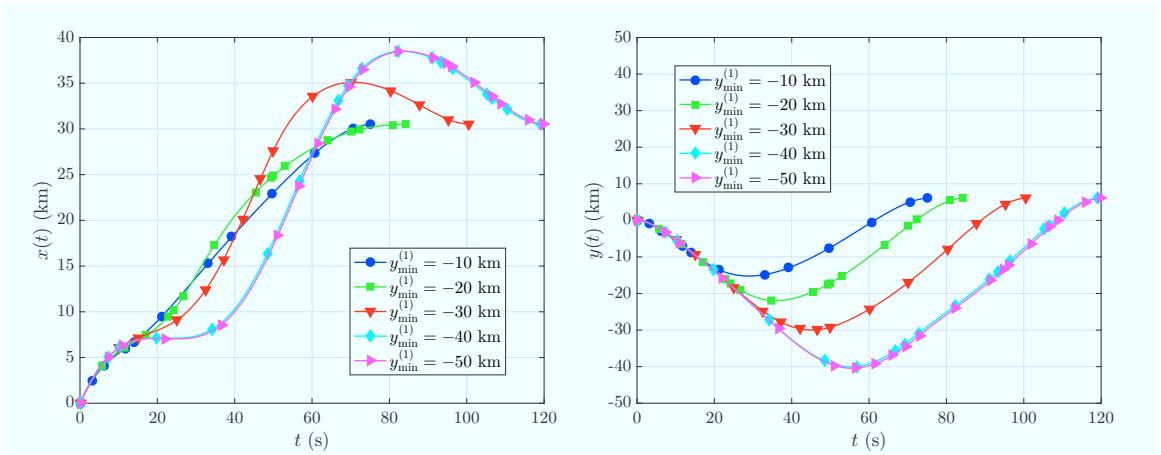

(a) Downtrack, $x(t)$, vs. t.

(b) Crosstrack, $y(t)$, vs. t.

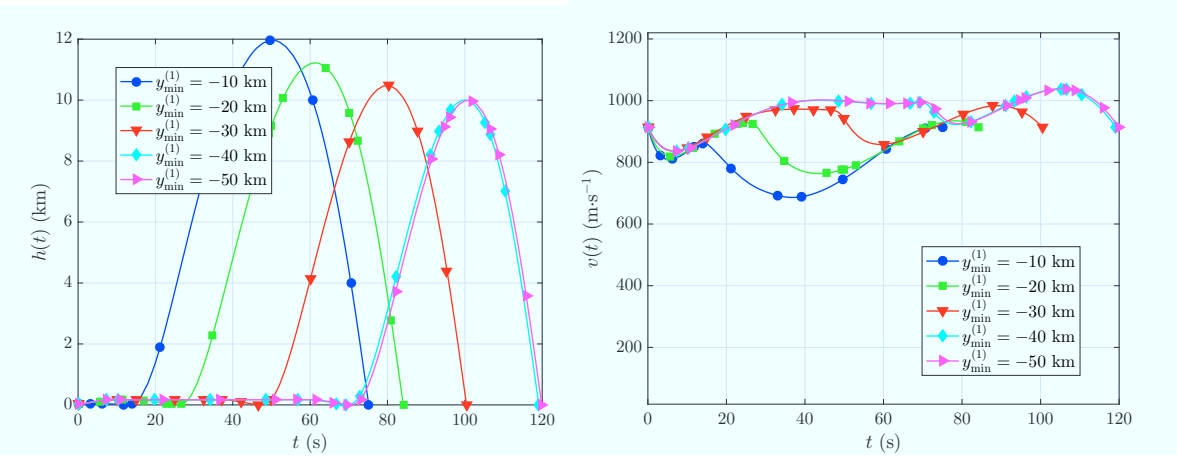

(c) Altitude, $h(t)$, vs. t.

(d) Speed, $v(t)$, vs. t.

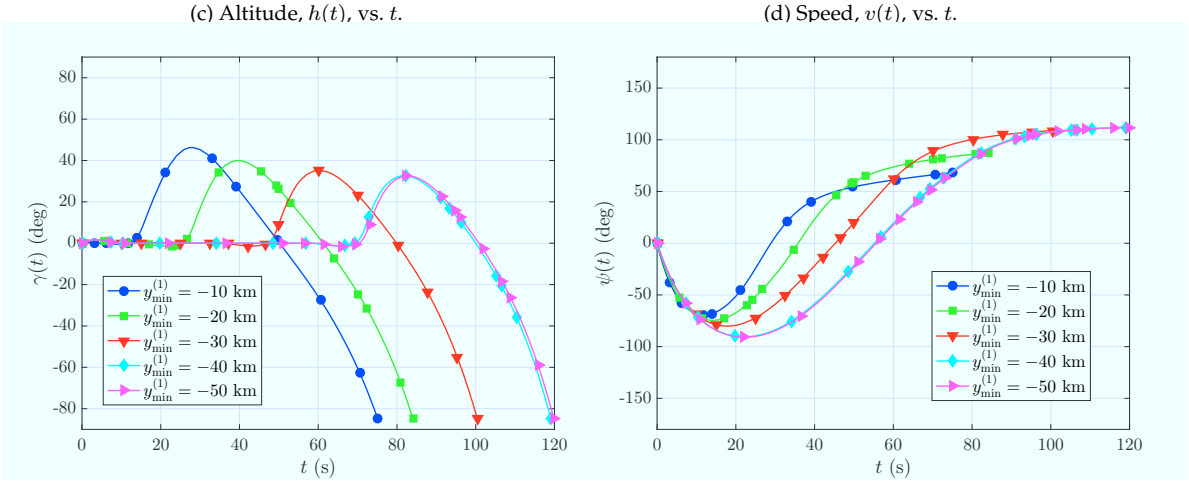

(e) Flight path angle, $\gamma(t)$, vs. t.

(f) Azimuth angle, $\psi(t)$, vs. t.

Figure 16: State solution, $(x(t), y(t), h(t), v(t), \gamma(t), \psi(t))$, vs. t of the optimal control problem described in Section III for a range of minimum and maximum allowable crossranges in the first phase with the cost function in Eq. (15) with an altitude constraint of $h_{\max}^{(1)} = 170$ m and a weighting factor of $W = 0.5$.

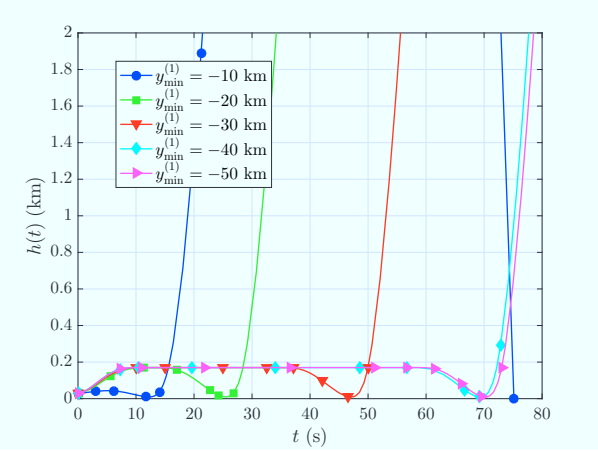

Figure 17: Altitude, $h(t)$, vs. t on solution to the optimal control problem described in Section III for a range of minimum and maximum allowable crossranges in the first phase with the cost function in Eq. (15) with an altitude constraint of $h_{\max}^{(1)} = 170$ m and a weighting factor of $W = 0.5$.

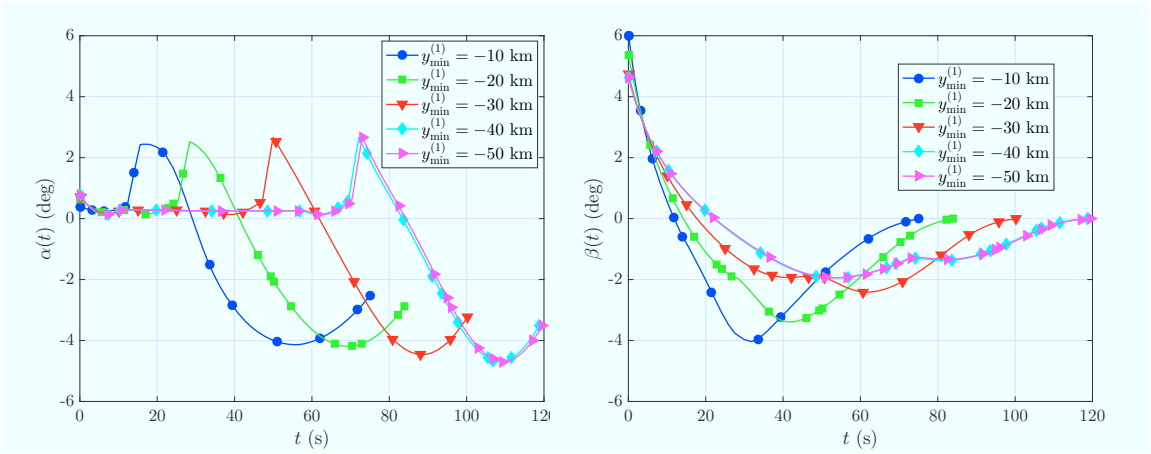

(a) Pitch angle, $\alpha(t)$, vs. t.

(b) Slip angle angle, $\beta(t)$, vs. t.

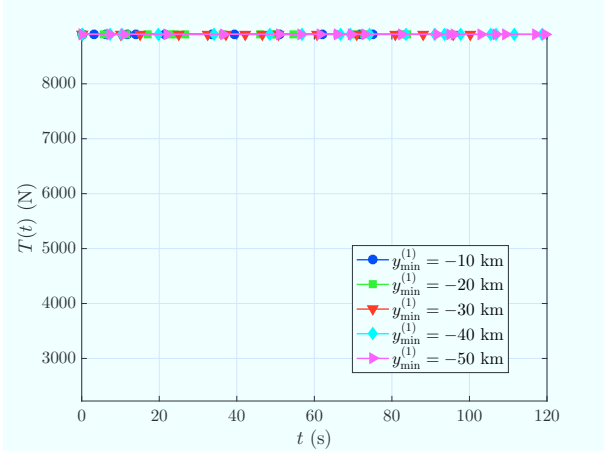

(c) Thrust magnitude, $T(t)$, vs. t.

Figure 18: Control solution, $(\alpha(t), \beta(t), T(t))$, vs. t of the optimal control problem described in Section III for a range of minimum and maximum allowable crossranges in the first phase with the cost function in Eq. (15) with an altitude constraint of $h_{\max}^{(1)} = 170$ m and a weighting factor of $W = 0.5$.

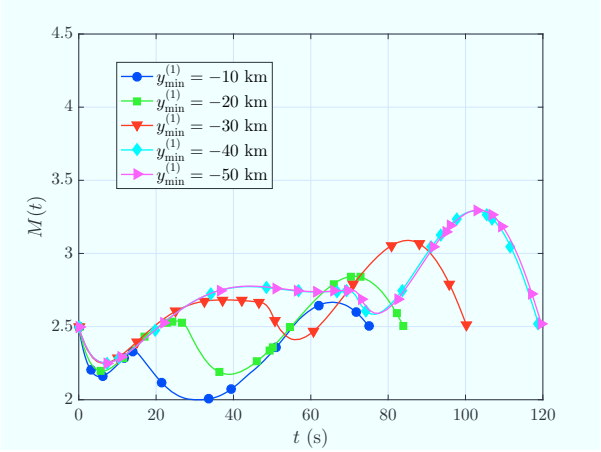

Figure 19: Mach number, $M(t)$, vs. t on solution to the optimal control problem described in Section III for a range of minimum and maximum allowable crossranges in the first phase with the cost function in Eq. (15) with an altitude constraint of $h_{\max}^{(1)} = 170$ m and a weighting factor of $W = 0.5$.

V. Conclusions

In the first part of this two-part study, the performance of a skid-to-turn vehicle is assessed. The optimal control problem is posed as a two-phase, bunt maneuver problem. To produce a bunt maneuver, additional altitude and crosstrack constraints are added to the first phase of the optimal control problem. The studies create an array of solutions to showcase how the state and control of the skid-to-turn vehicle model is affected by the added constraints in the first phase and the weight in the objective function. The two-phase optimal control problems are solved using $\mathbb{GPOPS} - \mathbb{II}$.[24] The results of this study identify that adding a second term that penalizes a higher bunt maneuver is effective in reducing the time and height of the vehicle in phase two during the bunt maneuver. Also, the maximum altitude constraint does not affect the solution of the optimal control problem greatly; however, a greater restriction on the crossrange flight of the vehicle produces a higher and longer bunt maneuver.

Acknowledgments

The authors acknowledge support for this research from the U.S. Office of Naval Research under grant N00014-15-1-2048, from the U.S. National Science Foundation under grants CBET-1404767, DMS-1522629, and CMMI-1563225, and from the Naval Air Warfare Center Weapons Division, China Lake, California under Contract No N68936-17-C-0011.

References

[1]Betts, J. T., *Practical Methods for Optimal Control and Estimation Using Nonlinear Programming*, SIAM Press, Philadelphia, 2nd ed., 2009.

[2]Gill, P. E., Murray, W., and Saunders, M. A., "SNOPT: An SQP Algorithm for Large-Scale Constrained Optimization," *SIAM Review*, Vol. 47, No. 1, January 2002, pp. 99–131.

[3]Gill, P. E., Murray, W., and Saunders, M. A., *User's Guide for SNOPT Version 7: Software for Large Scale Nonlinear Programming*, February 2006.

[4]Biegler, L. T. and Zavala, V. M., "Large-Scale Nonlinear Programming Using IPOPT: An Integrating Framework for Enterprise-Wide Optimization," *Computers and Chemical Engineering*, Vol. 33, No. 3, March 2008, pp. 575–582.

[5]Benson, D. A., Huntington, G. T., Thorvaldsen, T. P., and Rao, A. V., "Direct Trajectory Optimization and Costate Estimation via an Orthogonal Collocation Method," *Journal of Guidance, Control, and Dynamics*, Vol. 29, No. 6, November-December 2006, pp. 1435–1440.

[6]Garg, D., Patterson, M. A., Darby, C. L., Francolin, C., Huntington, G. T., Hager, W. W., and Rao, A. V., "Direct Trajectory Optimization and Costate Estimation of Finite-Horizon and Infinite-Horizon Optimal Control Problems via a Radau Pseudospectral Method," *Computational Optimization and Applications*, Vol. 49, No. 2, June 2011, pp. 335–358. DOI: 10.1007/s10589–00–09291–0.

[7]Garg, D., Patterson, M. A., Hager, W. W., Rao, A. V., Benson, D. A., and Huntington, G. T., "A Unified Framework for the Numer-

ical Solution of Optimal Control Problems Using Pseudospectral Methods," *Automatica*, Vol. 46, No. 11, November 2010, pp. 1843–1851. DOI: 10.1016/j.automatica.2010.06.048.

[8]Garg, D., Hager, W. W., and Rao, A. V., "Pseudospectral Methods for Solving Infinite-Horizon Optimal Control Problems," *Automatica*, Vol. 47, No. 4, April 2011, pp. 829–837. DOI: 10.1016/j.automatica.2011.01.085.

[9]Francolin, C. C., Hager, W. W., and Rao, A. V., "Costate Approximation in Optimal Control Using Integral Gaussian Quadrature Collocation Methods," *Optimal Control Applications and Methods*, Vol. 36, No. 4, July–August 2015, pp. 381–397.

[10]Darby, C. L., Hager, W. W., and Rao, A. V., "An hp-Adaptive Pseudospectral Method for Solving Optimal Control Problems," *Optimal Control Applications and Methods*, Vol. 32, No. 4, July–August 2011, pp. 476–502.

[11]Darby, C. L., Hager, W. W., and Rao, A. V., "Direct Trajectory Optimization Using a Variable Low-Order Adaptive Pseudospectral Method," *Journal of Spacecraft and Rockets*, Vol. 48, No. 3, May–June 2011, pp. 433–445.

[12]Patterson, M. A., Hager, W. W., and Rao, A. V., "A ph Mesh Refinement Method for Optimal Control," *Optimal Control Applications and Methods*, Vol. 36, No. 4, July–August 2015, pp. 398–421.

[13]Liu, F., Hager, W. W., and Rao, A. V., "Adaptive Mesh Refinement for Optimal Control Using Nonsmoothness Detection and Mesh Size Reduction," *Journal of the Franklin Institute*, Vol. 352, No. 10, October 2015, pp. 4081–4106.

[14]Liu, F., Hager, W. W., and Rao, A. V., "Adaptive Mesh Refinement for Optimal Control Using Using Decay Rates of Legendre Polynomial Coefficients," *IEEE Transactions on Control System Technology*, 2017, pp. 10.1109/TCST.2017.2702122.

[15]Hager, W. W., Hou, H., and Rao, A. V., "Lebesgue Constants Arising in a Class of Collocation Methods," *IMA Journal of Numerical Analysis*, Published Online: 24 December 2016. DOI: 10.1093/imanum/drw060.

[16]Hager, W. W., Hou, H., and Rao, A. V., "Convergence Rate for a Gauss Collocation Method Applied to Unconstrained Optimal Control," *Journal of Optimization Theory and Applications*, Vol. 169, 2016, pp. 801–824.

[17]Hager, W. W., Hou, H., and Rao, A. V., "Convergence Rate for a Radau Collocation Method Applied to Unconstrained Optimal Control," 2015, arXiv.org/abs/1508.03783.

[18]Hager, W. W., Hou, H., Mohapatra, S., and Rao, A. V., "Convergence Rate for an hp-Collocation Method Applied to Unconstrained Optimal Control," 2016, arXiv.org/abs/1605.02121.

[19]Hager, W. W., Mohapatra, S., and Rao, A. V., "Convergence Rate for a Gauss Collocation Method applied to Constrained Optimal Control," 2016, arXiv.org/abs/1607.02798.

[20]Farooq, A. and Limebeer, D. J. N., "Trajectory Optimization for Air-to-Surface Missiles with Imaging Radars," *Journal of Guidance, Control, and Dynamics*, Vol. 25, No. 5, September–October 2002, pp. 876–887.

[21]Farooq, A. and Limebeer, D. J. N., "Optimal Trajectory Regulation for Radar Imaging Guidance," *Journal of Guidance, Control, and Dynamics*, Vol. 28, No. 6, November–December 2005, pp. 1157–1170.

[22]Farooq, A. and Limebeer, D. J. N., "Optimal Trajectory Regulation for Radar Imaging Guidance," *Journal of Guidance, Control, and Dynamics*, Vol. 31, No. 4, July–August 2008, pp. 1076–1092.

[23]Stengel, R. F., *Optimal Control and Estimation*, Dover Publications, Mineola, New York, 1994.

[24]Patterson, M. A. and Rao, A. V., "$\mathbb{GPOPS}-\mathbb{II}$, A MATLAB Software for Solving Multiple-Phase Optimal Control Problems Using hp-Adaptive Gaussian Quadrature Collocation Methods and Sparse Nonlinear Programming," *ACM Transactions on Mathematical Software*, Vol. 41, No. 1, October 2014, pp. 1:1–1:37.

[25]Weinstein, M. J. and Rao, A. V., "Algorithm: ADiGator, a Toolbox for the Algorithmic Differentiation of Mathematical Functions in MATLAB," *ACM Transactions on Mathematical Software*, Accepted for Publication, May 2017.